Eur. Phys. J. C 5, 293–301 (1998)
DOI 10.1007/s100529800836

THE EUROPEAN PHYSICAL JOURNAL C

Production of hard photons and jets in deep inelastic lepton proton scattering at order $O(\alpha_s)$

G. Kramer[1], D. Michelsen[1,a], H. Spiesberger[2]

[1] II. Institut für Theoretische Physik[b], Universität Hamburg, D-22761 Hamburg, Germany
[2] Fakultät für Physik[b], Universität Bielefeld, D-33615 Bielefeld, Germany

Received: 18 December 1997 / Published online: 10 March 1998

Abstract. We calculate the $O(\alpha_s)$ corrections to the production of a hard and isolated photon accompanied by one or two jets in deep inelastic lepton nucleon scattering at HERA. Numerical results are presented and the potential of this process for studies of parton distribution functions is discussed.

1 Introduction

The production of hard photons in hadronic processes is an important testing ground for QCD. Since the photon does not take part in the strong interaction, it is a 'direct' probe of the hard scattering process. Direct photon production in γp [1] and in $p\bar{p}$ collisions [2] provides a means to determine the strong coupling constant α_s and has been used to extract information on the parton distributions, in particular the gluon density in the proton [3]. In e^+e^- annihilation [4], measurements of photon radiation in hadronic Z decays at LEP1 have provided important independent information on the electroweak couplings of *up* and *down* quarks to the Z boson [5,6]. Moreover, final states containing a photon are an important background for many searches for new physics and a good knowledge of the standard model predictions for direct photon production is therefore required.

At HERA, radiative deep inelastic scattering, $ep \to e\gamma X$, with photons collinear to the incoming electron has been used to obtain a measurement of the structure function F_2 at low values of the momentum transfer Q^2 [7]. Also the first observation of hard non-collinear photons at $Q^2 = 0$, *i.e.* in photoproduction has been reported recently [8]. With increasing luminosity this measurement is expected to contribute information on the parton content of the photon and the proton. By contrast, direct photon production at large Q^2 would be sensitive to the parton distributions in the proton only. The information obtained this way would be complementary to the F_2 measurement from inclusive deep inelastic scattering, since *up* and *down* quarks contribute with different weights. Typical cross sections for the production of hard photons in deep inelastic scattering with $Q^2 > 10$ GeV^2 are of the order of 10 pb. With a luminosity of 50 pb^{-1} one thus expects statistical uncertainties of the order of 5% and a measurement of differential cross sections seems feasible.

Whereas next-to-leading order calculations for direct photon production are available for photoproduction [1, 9], $p\bar{p}$ collisions [10], as well as for e^+e^- annihilation [11, 12], a corresponding calculation for deep inelastic ep scattering was still missing. In this work we study the $O(\alpha_s)$ corrections to the process $ep \to e\gamma X$ at large Q^2. Since hard photon production is a process of relative order $\alpha_e = 1/137$ with respect to the total deep inelastic scattering cross section, we expect sizable event rates only at moderately large Q^2 and restrict ourselves therefore to pure photon exchange, *i.e.* Z-exchange contributions are neglected. The calculations will be organized in such a way that the hadronic final state can be separated into $\gamma + (1+1)$-jet and $\gamma + (2+1)$-jet topologies (the remnant being counted as "+1" jet, as usual). Our approach is thus analogous to that in calculations of (2+1)- and (3+1)-jet cross sections in deep inelastic scattering where a gluon is replaced by a photon [13]. $\gamma + (2+1)$-jet events originate through the emission or absorption of a gluon. Therefore the ratio of $\gamma + (2+1)$-jet and $\gamma + (1+1)$-jet events is sensitive to the value of the strong coupling constant α_s and to the gluon distribution.

In addition to perturbative direct production, photons are also produced through the 'fragmentation' of a hadronic jet into a single photon carrying a large fraction of the jet energy [14]. This long-distance process is described in terms of the quark-to-photon and gluon-to-photon fragmentation functions. The necessity for taking into account non-perturbative contributions is signaled by the presence of singularities showing up in a perturbative calculation. These singularities are related to collinear photon-quark configurations. The factorization theorem of QCD guarantees that all singularities can be absorbed into well-defined universal parton-to-photon fragmenta-

[a] Now at IBM Deutschland, Informationssysteme GmbH
[b] Supported by Bundesministerium für Bildung, Wissenschaft, Forschung und Technologie, Bonn, Germany, Contracts 05 7BI92P (9) and 05 7HH92P (0)

tion functions, the remainder being calculable in perturbation theory.

In practice, a measurement of direct photon production is feasible only when isolation conditions are imposed on the observed photon in order to reduce various hadronic backgrounds, in particular from two-photon decays of π^0. The contribution from non-perturbative parton-to-photon fragmentation, being related to collinear photon emission from partons, can be reduced by isolation requirements, but is not completely removed. Again, in a perturbative calculation, this is related to the presence of singularities. In fact, if one tries to model the experimental isolation conditions by imposing cutoffs on parton-level jets, one can not exclude contributions due to soft quarks having emitted a hard collinear photon; the soft quark may appear only as part of a parton-level jet, but not as a separate, observable jet which can enter the isolation conditions[1]. The implementation of photon isolation is particularly non-trivial in a calculation including $O(\alpha_s)$ contributions since the isolation conditions affect the available phase space for gluon emission [19]. As a consequence, the parton-to-photon fragmentation functions may have to be modified for isolated photon production and higher-order corrections may turn out to be large and to require their resummation.

In the present work we adopt a simpler approach where the fragmentation contributions are ignored completely. The photon-quark collinear singularities then have to be removed by explicit parton-level cutoffs. The dependence of the final results on these cutoffs (discussed in Sect. 4 below) will indicate to what extent the quark-to-photon fragmentation function would contribute in a more systematic treatment.

2 The leading-order process

In leading order (LO), the production of photons in deep inelastic electron (positron) proton scattering is described by the quark (antiquark) subprocess

$$e(p_1) + q(p_3) \to e(p_2) + q(p_4) + \gamma(p_5) \tag{1}$$

where we have given the definition of the particle momenta in parentheses. The momentum of the incoming quark is a fraction of the proton momentum p_P: $p_3 = \xi p_P$. The proton remnant r carries the momentum

$$p_r = (1-\xi)p_P \tag{2}$$

and hadronizes into the remnant jet so that the process (1) gives rise to $\gamma+(1+1)$-jet final states. The momentum of the hadronic final state, *i.e.* the $(1+1)$-jet system, is $p_P + p_1 - p_2 - p_5$ and its invariant mass W is given by

$$W^2 = (p_P + p_1 - p_2 - p_5)^2. \tag{3}$$

We will use the well-known kinematic variables for deep inelastic scattering

$$Q^2 = -(p_1 - p_2)^2, \quad x = \frac{Q^2}{2p_P(p_1 - p_2)},$$
$$y = \frac{Q^2}{xs}, \quad s = (p_1 + p_P)^2, \tag{4}$$

determined by the momentum of the scattered lepton. Because of the presence of the photon in the final state, large Q^2 does not guarantee large W and we will have to require explicitly $W > W_{\min}$ in order to stay in the deep inelastic regime where a perturbative treatment can be expected to work. Apart from this, we will also apply cuts on the variables x, y and Q^2 since we ask for an observable scattered electron. These latter cuts remove direct photon production in photoproduction.

Both leptons and quarks emit photons. The subset of Feynman diagrams where the photon is emitted from the lepton ("leptonic radiation") is gauge invariant and can be treated separately. Similarly, the Feynman diagrams with a photon emitted from the quark line is called "quarkonic radiation". There is also a contribution from the interference of these two parts. For tests of QCD the interest is in those contributions where the photon is emitted from quarks and leptonic radiation is viewed as a background.

Radiative deep inelastic scattering appears as a contribution to QED radiative corrections (see for example [20] and references therein). In this case the emitted photon remains undetected and singularities due to soft and collinear photons have to be canceled by taking into account virtual $O(\alpha)$ corrections to non-radiative scattering $eq \to eq$. Here we are interested in events with an observable photon, *i.e.* we restrict ourselves to the case where the energy of the photon $E_\gamma = E_5$ is sufficiently large,

$$E_\gamma > E_{\gamma,\min}. \tag{5}$$

Also, the photon should be spatially separated from all other particles:

$$\theta_{\gamma,i} > \theta_{\rm sep}, \tag{6}$$

where $\theta_{\gamma,i}$ is the angle between the momenta of the photon and particle i $(= 1,2,3,4$ for the leading-order process (1) and similarly for the next-to-leading order processes specified in Sect. 3 below). In particular, the photon is not allowed to be emitted close to the beams:

$$\theta_{\min} < \theta_\gamma < \theta_{\max}. \tag{7}$$

These cuts remove all photonic infrared and collinear singularities. Instead of using the angle $\theta_{\gamma,i}$, photon separation from final state particles can also be imposed by cuts on the invariant masses

$$s_{ij} = (p_i + p_j)^2 \tag{8}$$

[1] The problem is most easily visible in $e^+e^- \to \gamma + 1$-jet, where already at leading order photon-jet isolation does not remove the photon-quark collinear singularity [12]. A next-to-leading order calculation [15] shows features typical for a next-to-next-to-leading order calculation. Measurements of the quark-to-photon fragmentation function in $e^+e^- \to \gamma + 1$-jet had been proposed in [16,17] and were described in [18].

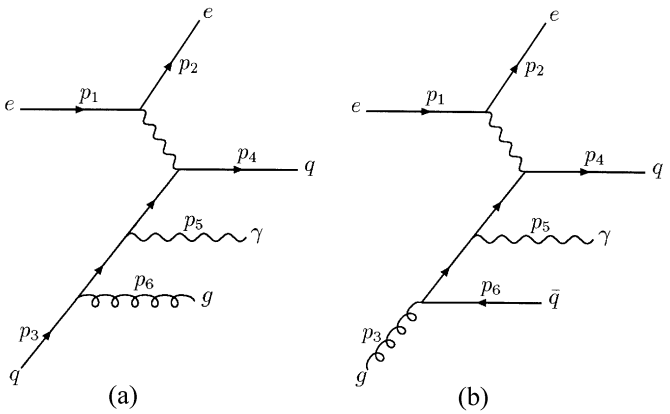

Fig. 1. Examples of Feynman diagrams for $eq \to eqg\gamma$ **a** and $eg \to eq\bar{q}\gamma$ **b** with the definition of momenta

or, normalized to the invariant mass of the hadronic final state,

$$y_{ij} = \frac{s_{ij}}{W^2}. \tag{9}$$

The condition

$$y_{5i} > y_0^\gamma \tag{10}$$

$(i = 2, 4, r)$ is more comfortable for the analytic calculation, but less suited to experimental requirements. Since we will perform the phase space integration with the help of Monte Carlo techniques, we are not restricted to one specific choice of isolation criteria, but we can apply a combination of the above cuts as will be described below.

At lowest order, each parton is identified with a jet and photon-parton isolation corresponds to the isolation of the photon from an observable jet. With isolation cuts, parton-to-photon fragmentation does not contribute at this order.

3 $O(\alpha_s)$ corrections

At next-to-leading order (NLO), processes with an additional gluon, either emitted into the final state or as incoming parton, have to be taken into account:

$$e(p_1) + q(p_3) \to e(p_2) + q(p_4) + \gamma(p_5) + g(p_6), \tag{11}$$

$$e(p_1) + g(p_3) \to e(p_2) + q(p_4) + \gamma(p_5) + \bar{q}(p_6), \tag{12}$$

where the definition of momenta is again shown in parentheses (see Fig. 1). In addition, virtual corrections (one-loop diagrams at $O(\alpha_s)$) to the process (1) have to be included.

The amplitude for purely leptonic radiation at order $O(\alpha_s)$ factorizes into a leptonic tensor for $e \to e\gamma\gamma^*$ and a hadronic tensor including next-to-leading order QCD corrections. Both parts are well-known and their combined contribution to deep inelastic scattering is included for example in the Monte Carlo program DJANGO6 [21]. For the $O(\alpha_s)$ corrections to quarkonic radiation and in particular the lepton-quark interference, a representation in terms of a leptonic and a hadronic tensor is not suitable. The corresponding complete matrix elements including the leptonic and hadronic vertex have been obtained with the help of `form` [22] and are given in [23].

Whereas the LO process leads to the appearance of events with a photon and one current jet, $\gamma + (1+1)$-jets, in higher orders additional jets can be produced: the processes (11, 12) contribute both to the $\gamma + (1+1)$-jetcross section, as well as to the cross section for $\gamma + (2+1)$-jets, depending on whether the quark-gluon or quark-antiquark pair in the final state appears as one single jet or as two separated jets. The two cases can be identified by comparing the scaled invariant masses of parton pairs with a jet resolution parameter y^J: two partons (i, j) with $i, j = 4, 6, r$ are supposed to lead to 2 jets if

$$y_{ij} > y^J. \tag{13}$$

Also the remnant r is treated as a parton and a quark, antiquark, or gluon in the final state is recombined with the remnant into one jet if $y_{ir} = \frac{1-\xi}{\xi} y_{i3}$ is smaller than y_0^J. Similarly, photon isolation can be imposed with the help of cuts on the scaled invariant masses.

In the phase space region where two jets can not be separated, the matrix elements become singular. These singularities appear when one of the partons becomes soft or when two partons become collinear to each other. The singularities can be assigned either to the initial state or to the final state (ISR: initial-state radiation, FSR: final-state radiation). The FSR singularities cancel against singularities from virtual corrections to the lower-order process. For the ISR singularities, this cancellation is incomplete and the remaining singular contributions have to be factorized and absorbed into renormalized parton distribution functions [24].

To accomplish this procedure, the singularities have to be isolated in an analytic calculation, e.g. with the help of dimensional regularization. The application of dimensional regularization is, however, not feasible for the complete cross section of the higher-order processes. Therefore we use the so-called phase-space slicing method [25] to separate those regions in the 4-particle phase space which give rise to singular contributions. A separation cut y_0^J is applied to the scaled invariant masses y_{ij} and chosen small enough, such that the calculation can be simplified by neglecting terms of the order $O(y_0^J)$. Contributions from phase space regions where one of the y_{ij} is smaller than y_0^J are singular and have to be combined with the one-loop corrections to obtain a finite result. The sum of these two contributions defines the cross section for events where two partons are recombined into a parton-level jet (parton-level $(1+1)$-jet events). The contributions where all y_{ij} are bigger than y_0^J are related to final states with three separate partons (parton-level $(2+1)$-jet events). The latter are free of singularities and can be calculated with the help of Monte Carlo techniques.

As known from similar calculations (e.g., for the (non-radiative) jet cross sections in DIS [26]), the phase space slicing parameter y_0^J has to be chosen very small, of the order of 10^{-3} or smaller, in order to allow for the neglect of

terms of order $O(y_0^J)$. Therefore, y_0^J can not be identified with the y-cut of a jet algorithm applied in an experimental analysis. There, due to experimental restrictions, y cannot be reduced to values below $O(10^{-3})$. In addition, a fixed-order calculation may give unphysical, *i.e.* negative $(1+1)$-jet cross sections for too small values of y (see the curves labeled with S in Figs. 2a and 3a below). The Monte Carlo approach, however, allows to apply a jet algorithm to the parton-level events, *i.e.* to recombine 2 partons in the parton-level $(2+1)$-jet events according to a jet algorithm using y-cuts y^J for the separation of jet pairs (similarly: y^γ for the separation of a jet and a photon) with values as appropriate for the given experimental situation.

The calculation thus proceeds through two subsequent steps: First, phase space slicing is applied with a small y-cut y_0^J of the order of $\lesssim 10^{-3}$ to accomplish the cancellation of singularities. This step relies on analytic calculations. Secondly, a jet algorithm is applied with experimentally realizable, *i.e.* large enough values y^J and y^γ of the order of $0.01 - 0.1$. The second step is performed during the Monte Carlo integration.

The singular contributions for the process $eq \to eqg\gamma$ involve the following factors

$$\left\{ \frac{1}{y_{36}}, \frac{1}{y_{46}} \right\}, \tag{14}$$

those for $eg \to eq\bar{q}\gamma$ contain the factors

$$\left\{ \frac{1}{y_{36}}, \frac{1}{y_{34}} \right\}. \tag{15}$$

Terms containing $1/y_{3i}$, *i.e.* the momentum p_3 of the incoming parton, are associated to initial-state singularities, terms that do not, to final-state singularities. Contributions involving the product of an ISR and an FSR factor, as for example the factor $1/y_{36}y_{46}$, can be separated by partial fractioning,

$$\frac{1}{y_{ij}y_{ik}} = \frac{1}{y_{ij}} \frac{1}{y_{ij}+y_{ik}} + \frac{1}{y_{ik}} \frac{1}{y_{ij}+y_{ik}}, \tag{16}$$

so that all singular contributions can be associated either to the initial state or to the final state. Note that the denominator $y_{ij} + y_{ik}$ introduced by partial fractioning can become zero only if both $y_{ij} = 0$ and $y_{ik} = 0$ at the same time; since configurations where all three partons 3, 4, and 6 are collinear with each other are excluded by the cut on W, this is possible only for $p_i = 0$. Therefore, for a contribution containing the pole factor $1/y_{ij}$, we can separate the phase space into three regions:

- $y_{ij} < y_0^J$. This region contains the infrared singularity at $y_{ij} = y_{ik} = 0$, as well as the collinear singularity at $y_{ij} = 0$, $y_{ik} > 0$ and leads to singular contributions, *i.e.* $1/\epsilon$ and $1/\epsilon^2$ poles in dimensional regularization. The double-poles $1/\epsilon^2$ and parts of the single-poles $1/\epsilon$ cancel with corresponding singular contributions from virtual corrections. The remaining $1/\epsilon$-pole contributions are associated to the initial state, can be factorized, and are absorbed by renormalizing the parton distribution functions. The analytical integration over this phase space region is performed with the approximation of small y_0^J, *i.e.* neglecting terms of $O(y_0^J)$. This contribution will be denoted by "S" (singular) below.
- $y_{ij} \geq y_0^J$ and $y_{ik} \geq y_0^J$ with only parton-level γ+(2+1)-jet events, denoted by "R" (real corrections);
- $y_{ij} \geq y_0^J$ and $y_{ik} < y_0^J$. Here, the result is non-singular (therefore denoted by "F", finite) but does not vanish with $y_0^J \to 0$, contrary to naive expectations. Its contribution is calculated numerically. It is non-negligible in particular for terms related to ISR singularities.

The integrals needed for the singular contributions are written in a Lorentz-invariant form as tensor integrals which can be reduced to a few basic scalar integrals with the help of analytic programs like `mathematica` or `form`. More details are given in [23]. The remaining phase space integrations are performed with the help of Monte Carlo techniques. The three contributions S, R, and F are treated separately, each with appropriate mappings of the respective integration variables to improve the numerical stability of the calculation.

As discussed in the introduction, in the present work we do not factorize and subtract those photon-parton collinear singularities which have to be absorbed into parton-to-photon fragmentation functions. Instead, we remove all singular contributions by keeping isolation cuts at the parton level. As stated in the introduction, care has to be taken that the isolation criteria do not restrict the phase space for gluon emission since this would destroy the cancellation of singular contributions. Therefore, in the first step of the calculation described above, we require the photon to be isolated from the quark (antiquark) by the cut

$$y_{5i} > y_0^\gamma \tag{17}$$

with $i = 3, 4$ for $eq \to eqg\gamma$ and $i = 4, 6$ for $eg \to eq\bar{q}\gamma$. The cut is not applied to photon-gluon pairs which is possible since gluons do not emit photons and there is no singularity related to $y_{g\gamma}$. This definition of photon isolation at the parton level introduces an unphysical parameter (y_0^γ). The sensitivity to y_0^γ can be reduced by applying, in the second step of the calculation, photon isolation with respect to jets described by cutoff parameters which can be used in the same way in the experimental analysis. In order to have some freedom when modeling these physical isolation criteria we choose a small value for y_0^γ. The dependence on y_0^γ will be discussed below.

4 Numerical results

The results discussed in the following are obtained for energies and cuts appropriate for the HERA experiments: the energies of the incoming electron (positron) and proton are $E_e = 27.5$ GeV, $E_P = 820$ GeV and

$$\begin{gathered} Q^2 \geq 10 \text{ GeV}^2, \quad W \geq 10 \text{ GeV}, \\ 0.001 \leq x \leq 0.5, \quad 0.05 \leq y \leq 0.99, \\ p_\gamma^T \geq 5 \text{ GeV}, \quad 90^\circ \leq \theta_\gamma \leq 170^\circ, \quad \theta_{\gamma e} \geq 10^\circ. \end{gathered} \tag{18}$$

Note that the emission angle of the photon, θ_γ, measured with respect to the incoming electron in the HERA laboratory frame, is restricted to the hemisphere $\theta_\gamma \geq 90^\circ$ since photon production with $\theta_\gamma < 90^\circ$ is dominated by 'uninteresting' leptonic radiation. The parton distribution functions are taken from [28] (MRS(A)).

The events generated during Monte Carlo integration are γq, γqg or $\gamma q\bar{q}$ events. A simple event analysis is applied to obtain $\gamma + (1+1)$-jet and $\gamma + (2+1)$-jet event samples. The event analysis consists of two parts: the first part serves to identify the number of jets according to a conventional jet algorithm; the second part treats photon isolation. For simplicity we choose a jet definition using the normalized invariant masses y_{ij}. Since for small $\xi \geq x$ the momentum of the remnant and thus y_{ir} can be large even for partons with small transverse momentum, we first remove low-p^T partons before recombining partons to jets. Explicitly we apply the following conditions:

(1) A final state parton (quark or gluon) is recombined with the remnant if its transverse momentum is below a cutoff:

$$p_i^T < p_{\min}^T = 1 \text{ GeV}, \quad i = 4, 6. \tag{19}$$

(2) Two partons are recombined into one jet if

$$y_{ij} < y^J \quad \text{for} \quad i, j = 4, 6, r \tag{20}$$

and all quarks, antiquarks and gluons as well as the proton remnant are taken into account when forming jets. If several pairs of partons have y_{ij} below y^J, the pair with the smallest y_{ij} is recombined first. Several prescriptions for the recombination are possible: the energy and 3-momentum of a jet (ij) obtained from pairing partons i and j can be obtained by

$$E_{ij} = \alpha(E_i + E_j), \quad \mathbf{p}_{ij} = \beta(\mathbf{p}_i + \mathbf{p}_j). \tag{21}$$

For example in the E-scheme one chooses $\alpha = \beta = 1$; in the P-scheme one has $\alpha = |\mathbf{p}_i + \mathbf{p}_j| / (E_i + E_j)$, $\beta = 1$ instead. Since the present calculation is of first order in α_s, the recombination has not to be iterated. However, the different recombination prescriptions become relevant when photon isolation with respect to jets is imposed. In addition, the cut on low-p_T partons or parton-pairs (19) is affected if a recombination prescription with $\beta \neq 1$ is used. Our numerical results will be given for the P-scheme.

(3) Finally, an event is accepted only if the photon is separated from the jets or if the photon is accompanied by hadronic energy less than a specified amount, *i.e.* we exclude events with

$$y_{\gamma j} < y^\gamma \quad \text{and} \quad E_j > \epsilon\,(E_j + E_\gamma) \tag{22}$$

where j denotes any jet (*i.e.*, parton or pair of partons) remaining after steps (1) and (2) of the event analysis.

We keep the possibility to use different values for the y-cuts applied to purely hadronic jets and to jets containing the photon. In practice, y^J and y^γ are taken equal with a typical value 0.03. For the photon isolation parameter ϵ we will take the value 0.1 as used in experimental analyses [8]. Apart from being experimentally unrealistic, the value $\epsilon = 0$ is theoretically not allowed since (22) with $\epsilon = 0$ would restrict the phase space for soft partons and consequently destroy the cancellation of corresponding singularities.

We start with demonstrating the consistency of our approach by showing the dependence of the $\gamma + (1+1)$-jet cross section on the phase space slicing cut y_0^J. Figures 2 and 3 show the dependence of the total and partial cross sections for $\gamma + (1+1)$-jet events. For $q(\bar{q})$-initiated processes, the separate contributions S and R depend on $\log^2 y_0^J$ (see Fig. 2a) and the finite contribution F is not negligible. In this case the sum is numerically stable in the range $10^{-5} \lesssim y_0^J \lesssim 10^{-3}$; for smaller values the numerical precision decreases and for larger values the error from neglected terms of order $O(y_0^J)$ is not negligible. The calculation of g-initiated contributions can be performed with much smaller uncertainties and for much smaller values of y_0^J, as seen in Fig. 3 since here the dependence on $\log y_0^J$ is only linear. Also, the finite contribution is negligible for diagrams with incoming gluons. The dependence on y_0^J at large values above $\simeq 10^{-3}$ is slightly stronger in this case than for $q(\bar{q})$-initiated contributions since terms of order $O(y_0^J)$ are relatively more important. In the following we fix y_0^J at the value 10^{-4}.

Figure 4 shows the residual dependence of the cross sections for γ+(1+1)-jets on the parton-level photon isolation cut y_0^γ, separately for (anti)quark and gluon-initiated processes. The y_0^γ-dependence is weak for the case with incoming (anti)quarks showing that the isolation criteria efficiently reduce the sensitivity to the phase space region where the non-perturbative parton-to-photon fragmentation functions would contribute. For the g-initiated processes, the sensitivity to y_0^γ is larger. In this case all final-state partons (q and $\bar{q}$) can emit a photon. Since the isolation condition is applied to jets, the singularity associated to configurations with soft (anti)quarks having emitted a hard collinear photon is removed only with the help of the parton-level cut (17). For processes with incoming quarks, only a small subset of diagrams leads to singularities for similar configurations. We choose $y_0^\gamma = 10^{-4}$ in the following. This value is small enough compared with experimentally realistic values for $y^\gamma \gtrsim O(10^{-2})$ so that contributions where a quark or an antiquark determines the momentum of a jet, become insensitive to y_0^γ. Also, much larger values would lead to an unphysical negative cross section for the g-initiated subprocess. In a more systematic treatment, the y_0^γ-dependent terms in our calculation would be replaced by contributions from parton-to-photon fragmentation functions. In our present approach, however, the unwanted dependence on y_0^γ has to be viewed as an unavoidable source of a theoretical uncertainty. The $\gamma+(1+1)$-jetcross section at $Q^2 \lesssim 100$ GeV^2 is affected by this at the level of 20% (see Fig. 6 below). At larger Q^2, the influence of the y_0^γ-dependent gluon-initiated contribution is reduced[2].

[2] This can be compared with the case of $e^+e^- \to \gamma$+hadrons where the total cross section has little sensitivity to the parton-

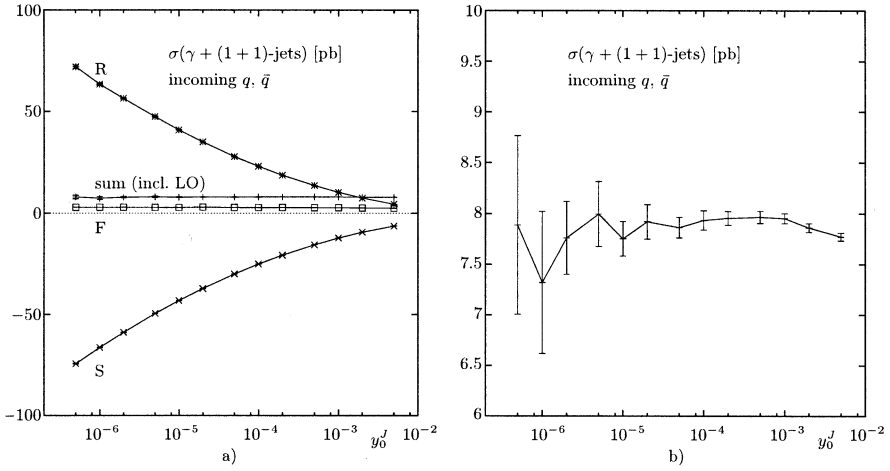

Fig. 2. Dependence of the $\gamma + (1 + 1)$-jet cross section on the phase space slicing cut y_0^J for incoming quarks and antiquarks ($y_0^\gamma = 10^{-4}$, $y^\gamma = y^J = 0.03$). **a** shows the separate contributions and the sum = R + S + F + LO. **b** shows the sum of all contributions, including the leading-order cross section, on a larger scale

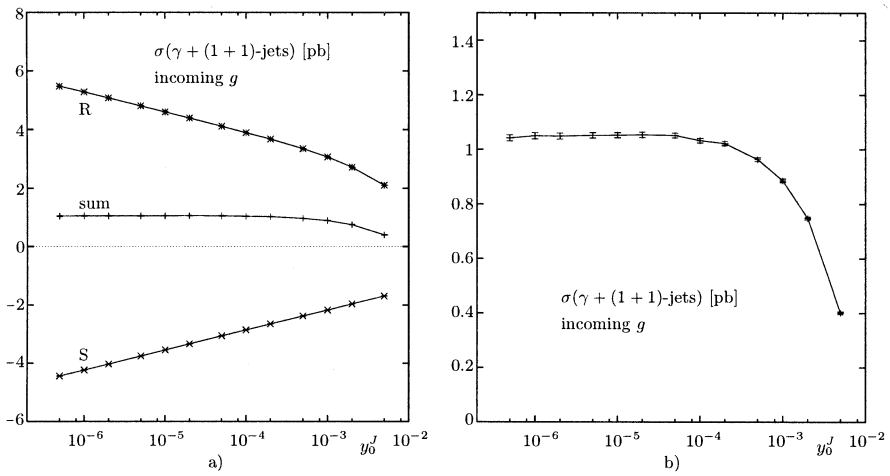

Fig. 3. Dependence of the $\gamma + (1 + 1)$-jet cross section on the phase space slicing cut y_0^J for incoming gluons ($y_0^\gamma = 10^{-4}$, $y^\gamma = y^J = 0.03$). **a** shows the separate contributions and the sum = R + S. **b** shows the sum of all contributions on a larger scale

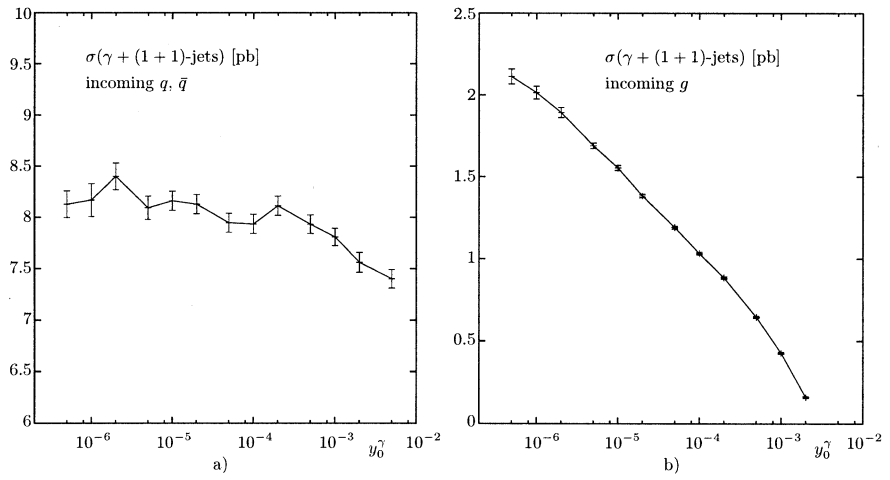

Fig. 4. Dependence on the infrared cutoff parameter y_0^γ of the $\gamma + (1 + 1)$-jet cross section for incoming (anti)quarks **a** and gluons **b** ($y_0^J = 10^{-4}$, $y^\gamma = y^J = 0.03$)

In Fig. 5 we show the differential cross section $d\sigma/d\theta_\gamma$ (sum of $\gamma + (1 + 1)$-jets and $\gamma + (2 + 1)$-jets) in the range $10^\circ \leq \theta_\gamma \leq 175^\circ$. Apart from the extended range of photon emission angles all cuts given in (18) are applied. The majority of photons is produced with small angles, *i.e.* close to the direction of the incoming lepton. For leptonic radiation, QCD corrections reduce the cross section by $\sim 10\%$ for the phase space region under consideration. By contrast, at large emission angles, dominated by quarkonic radiation, the cross section receives positive QCD corrections. In the following we restrict ourselves again to this "signal" region $\theta_\gamma \geq 90^\circ$, *i.e.* the proton hemisphere in the HERA laboratory system.

level photon isolation cut for not too large y, but the $\gamma + 1$-jet rate has a non-negligible dependence on y_0^γ [27].

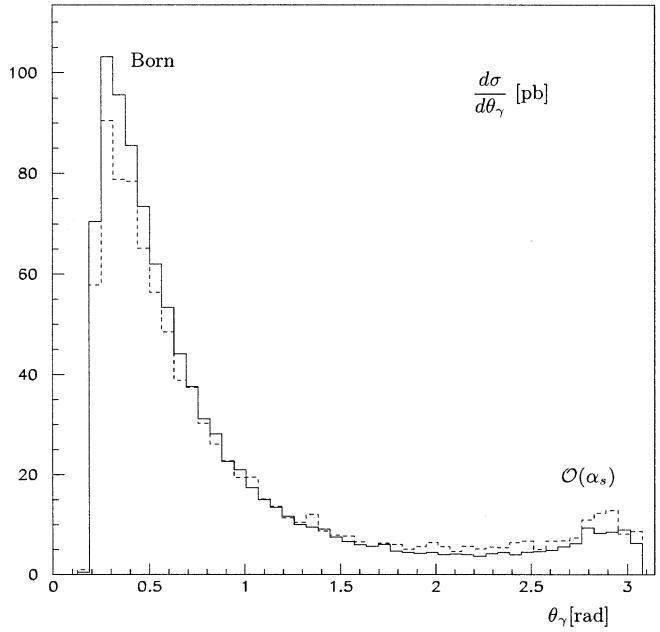

Fig. 5. Differential cross section $d\sigma/d\theta_\gamma$ for $ep \to e\gamma + (1+1)$-jets and $ep \to e\gamma + (2+1)$-jets with $y^J = y^\gamma = 0.03$. *Full histogram*: lowest order, *dashed histogram*: including $O(\alpha_s)$ corrections. Cuts are explained in the text

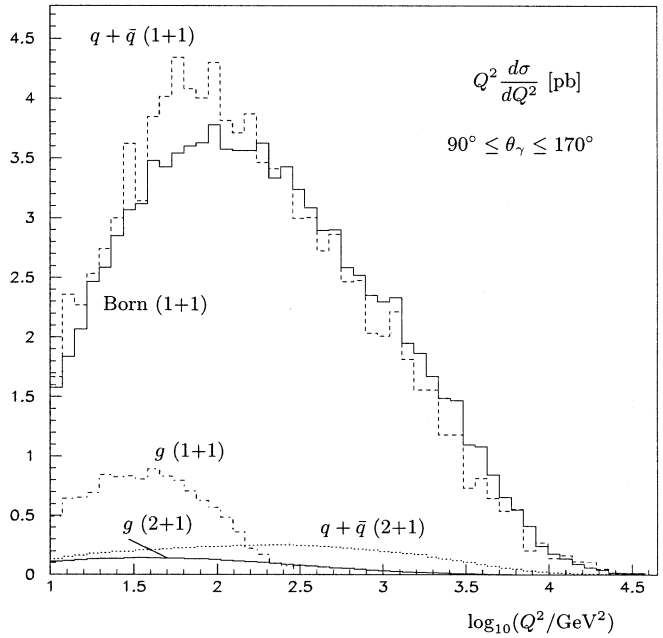

Fig. 6. Differential cross section $Q^2 d\sigma/dQ^2$ for $ep \to e\gamma + (n+1)$-jets with $y^J = y^\gamma = 0.03$. *Upper full histogram*: lowest order, *dashed histogram*: contribution from incoming (anti)quarks to $\gamma + (1+1)$-jets, *dotted histogram*: contribution from incoming (anti)quarks to $\gamma + (2+1)$-jets, *dash-dotted histogram*: incoming gluons for $\gamma + (1+1)$-jets, *lower full histogram*: incoming gluons for $\gamma + (2+1)$-jets. Photons are restricted to $90° \le \theta_\gamma \le 170°$ and other cuts are explained in the text

The Q^2-dependence in this restricted phase space region is shown in Fig. 6. The cross section is shown separately for $q(\bar{q})$-initiated and gluon-initiated contributions giving rise to $\gamma + (1+1)$-jet and $\gamma + (2+1)$-jet events using $y^J = y^\gamma = 0.03$. The $\gamma + (1+1)$-jet contribution is dominant for these y-cut values with a maximum in the lower Q^2 range, whereas the cross section for $\gamma + (2+1)$-jet events is flatter and extends to larger Q^2. Incoming gluons contribute only roughly 10% to the total cross section. Since the distributions for incoming quarks and incoming gluons are not very different, it seems difficult to utilize radiative deep inelastic scattering for a measurement of the gluon distribution. We also checked that using other parametrizations of parton distribution functions (like those of [29]) do not lead to significantly different shapes of distributions. Only the total cross sections vary by $O(10-15\%)$.

The rate of $\gamma + (2+1)$-jet events,

$$R_{\gamma,2+1} = \frac{\sigma(\gamma + (2+1)\text{−jets})}{\sigma(\gamma + (1+1)\text{−jets}) + \sigma(\gamma + (2+1)\text{−jets})}, \tag{23}$$

increases towards smaller values of y^J (see Fig. 7) and becomes equal to the $\gamma + (1+1)$-jet rate at $y^J \lesssim 10^{-3}$, the precise value depending on y^γ. The dependence on y^γ is weaker; in particular, for $y^\gamma \gtrsim 0.02$ the $\gamma + (2+1)$-jet rate is almost independent on y^γ. The reduction of the cross sections with increasing y^γ is stronger for $\gamma + (2+1)$-jet events at large values of y^J than at small y^J, relative to the $\gamma + (1+1)$-jet cross section, *i.e.* the ratio $R_{\gamma,2+1}$ increases with increasing y^γ at large y^J whereas it decreases with increasing y^γ at small y^J. For completeness we present the

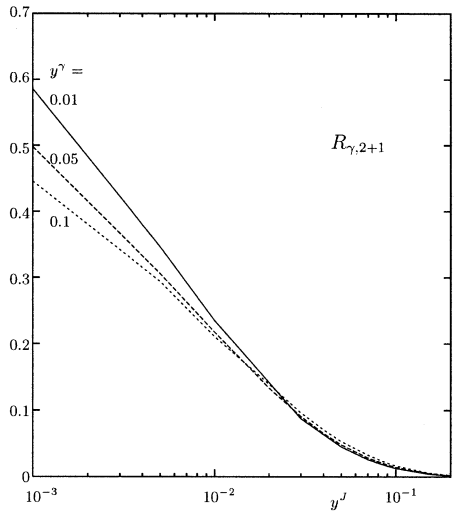

Fig. 7. $\gamma + (2+1)$-jet rate $R_{\gamma,2+1}$ as a function of the jet cut y^J for three different values of the photon isolation cut y^γ

y-cut dependence of the $\gamma + (1+1)$-jet and $\gamma + (2+1)$-jet cross sections in Fig. 8. Note that also the total cross section has a dependence on y^J, as can be seen from the sum of the results shown in Figs. 8a and b. The jet algorithm not only defines the classification of the hadronic final state into $\gamma + (1+1)$-jet or $\gamma + (2+1)$-jet events, but also affects the overall phase space boundaries: smaller values of y^J allow the jets to be closer to the remnant

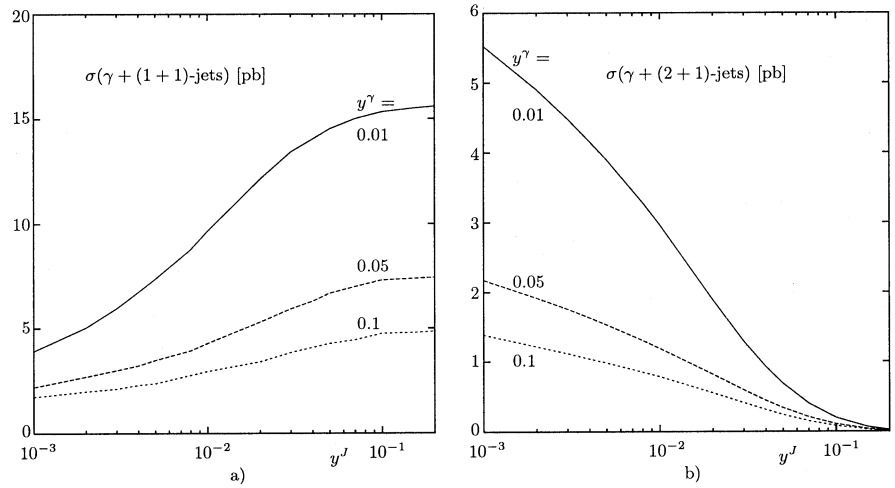

Fig. 8. $\gamma + (1+1)$-jet and $\gamma + (2+1)$-jet cross sections as a function of jet cut and photon isolation

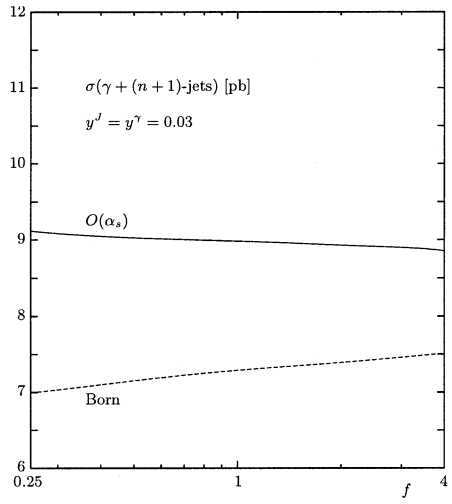

Fig. 9. Dependence on the renormalization and factorization scales $\mu_F^2 = \mu_R^2 = fQ^2$ of the total cross section (*i.e.*, the sum of $\gamma + (1+1)$-jets and $\gamma + (2+1)$-jets) for $y^J = y^\gamma = 0.03$

jet so that the cut against low-p^T partons has a stronger effect.

The leading order cross section depends on a factorization scale μ_F via the scale entering the parton distribution functions $q_i(x, \mu_F^2)$. At next-to-leading order, there is an explicit scale dependence in the $\gamma + (1+1)$-jet cross section through factorization of the initial state singularities which partly compensates the scale dependence from the parton distribution functions. In addition, the explicit factor α_s depends on the renormalization scale. For simplicity we identify the two scales, which could in principle be chosen independently from each other. Figure 9 shows the scale dependence of the leading-order and the next-to-leading order cross sections where we have used $\mu_F^2 = \mu_R^2 = fQ^2$. Varying f between 0.25 and 4, the total cross section for $ep \to e\gamma X$ shows good stability within a few percent. Also from this figure one can infer that the $O(\alpha_s)$ corrections vary between 20 and 30%. A 5% measurement of the cross section would therefore correspond to a 20 to 30% measurement of α_s, assuming negligible uncertainties from parton distribution functions.

Radiative ep scattering is complementary to usual deep inelastic scattering since up and down-type quarks contribute with different weights to the cross sections. In the usual structure function F_2, the sums of u- and d-type quarks, $U = u + c + \bar{u} + \bar{c}$ and $D = d + s + b + \bar{d} + \bar{s} + \bar{b}$ enter with the relative factors $e_u^2 : e_d^2 = 4 : 1$ whereas for the contribution from quarkonic radiation to $ep \to e\gamma X$ this ratio is $e_u^4 : e_d^4 = 16 : 1$. In principle, a common analysis of non-radiative and radiative scattering performed with high enough precision, would allow a determination of U and D separately. We therefore investigated the dependence of the total cross section for $ep \to e\gamma X$ on the ratio U/D. In order to keep the well-constrained structure function F_2 unchanged, we modified the parton distributions by the following prescription:

$$D \to \delta_d D,$$
$$U \to \left(1 + \frac{1-\delta_d}{4(U/D)}\right) U. \tag{24}$$

By this the combination $e_u^4 U + e_d^4 D$ is replaced with $[1 + 3(1-\delta_d)/(1+16U/D)] \times (e_u^4 U + e_d^4 D)$. With $U/D \simeq 1.5$, a typical value at $x \simeq 0.1$, one expects a 12% reduction for $\delta_d = 2$ and a 6% enhancement for $\delta_d = 0.5$. In fact, the true change of the cross section is smaller (-5.7% and $+2.3\%$ with the cuts (18)) since additional contributions from leptonic radiation and quark-lepton interference, which are not proportional to the fourth power of the quark charges, are not negligible even in the 'signal' region $\theta_\gamma \geq 90°$. It thus seems unlikely that with respect to a determination of U/D radiative deep inelastic scattering could become competitive with classical analyses like that of the difference of proton and neutron cross sections or the W charge asymmetry in $p\bar{p} \to W^\pm + X$.

5 Summary

We have described a first next-to-leading order calculation of isolated photon production in ep scattering at large Q^2.

Apart from providing a sound basis for testing QCD in direct photon production, our results improve the knowledge of standard model predictions as a source of background for searches for new physics. We have discussed numerical results for $\gamma + (1 + 1)$-jet and $\gamma + (2 + 1)$-jet cross sections at HERA. Corresponding measurements will provide valuable information that will allow to further constrain parton distribution functions, in particular when combined with results from other experiments. It still has to be investigated which kinematical variable would be best suited to obtain the highest sensitivity on the gluon distribution, the U/D ratio, or the strong coupling constant α_s. For example, in photoproduction the distributions with respect to the photon rapidity or photon transverse momentum (in the HERA laboratory or in the $\gamma^* p$ center-of-mass frame) turned out to be good choices. One should also expect that the theoretical uncertainties due to the parton-level cutoff y_0^γ could be further reduced by optimizing the analysis with respect to kinematical cuts, the jet algorithm (e.g., a cone algorithm as used in the study of $(2 + 1)$- or $(3 + 1)$-jet events at HERA [30]) and modified photon isolation prescriptions (e.g., the so-called "democratic" clustering procedure [16]).

Acknowledgements. We wish to thank D. Graudenz for useful discussions.

References

1. P. Aurenche et al., Z. Phys. C24 (1984) 309; P. Aurenche et al., Phys. Rev. D39 (1989) 3275; P. Aurenche et al., Z. Phys. C56 (1993) 589
2. J.F. Owens, Rev. Mod. Phys. 59 (1987) 465; and references therein
3. A.D. Martin, R.G. Roberts, W.J. Stirling, Phys. Lett. B387 (1996) 419
4. Proc. Workshop on Photon Radiation from Quarks, Annecy 1991, CERN Yellow Report 92-04; DELPHI Collaboration: P. Abreu et al., Z. Phys. C53 (1992) 555; Z. Phys. C69 (1995) 1; OPAL Collaboration: P.D. Acton et al., Z. Phys. C58 (1993) 405; R. Akers et al., Z. Phys. C67 (1995) 15; ALEPH Collaboration: D. Buskulic et al., Z. Phys. C57 (1993) 17; L3 Collaboration: O. Adriani et al., Phys. Lett. B292 (1992) 472; Phys. Lett. B301 (1993) 136
5. E. Laermann, T.F. Walsh, I. Schmitt, P.M. Zerwas, Nucl. Phys. B207 (1982) 205; P. Mättig, W. Zeuner, Z. Phys. C52 (1991) 31
6. OPAL Collaboration, G. Alexander et al., Phys. Lett. B264 (1991) 219; P.D. Acton et al., Z. Phys. C58 (1993) 405; DELPHI Collaboration, P. Abreu et al., Z. Phys. C69 (1995) 1; L3 Collaboration, O. Adriani, Phys. Lett. B301 (1993) 136
7. H1 Collaboration, T. Ahmed et al., Z. Phys. C66 (1995) 529; H1 Collaboration, S. Aid et al., Nucl. Phys. B470 (1996) 3; ZEUS Collaboration, M. Derrick et al., Z. Phys. C69 (1996) 607
8. ZEUS Collaboration, J. Breitweg et al., DESY 97-146, (subm. to Phys. Lett. B)
9. L.E. Gordon, J.K. Storrow, Z. Phys. C63 (1994) 581; L.E. Gordon, W. Vogelsang, Phys. Rev. D52 (1995) 58; L.E. Gordon, ANL-HEP-CP-97-41 (hep-ph/9706355)
10. H. Baer, J. Ohnemus, J.F. Owens, Phys. Rev. D42 (1990) 61; P. Aurenche et al., Nucl. Phys. B399 (1993) 34; L.E. Gordon, W. Vogelsang, Phys. Rev. D50 (1994) 1901; M. Glück, L.E. Gordon, E. Reya, W. Vogelsang, Phys. Rev. Lett. 73 (1994) 388; W. Vogelsang, A. Vogt, Nucl. Phys. B453 (1995) 334
11. G. Kramer, B. Lampe, Phys. Lett. B269 (1991) 401
12. G. Kramer, H. Spiesberger, Proc. Workshop on Photon Radiation from Quarks, Annecy 1991, Cern Yellow Report 92-04, p. 26; E.W.N. Glover, W.J. Stirling, Phys. Lett. B295 (1992) 128; Z. Kunszt, Z. Trocsanyi, Nucl. Phys. B394 (1993) 139
13. D. Graudenz, PhD thesis, Hamburg 1990; Phys. Rev. D49 (1994) 3291; T. Brodkorb, E. Mirkes, Z. Phys. C66 (1996) 141; E. Mirkes, D. Zeppenfeld, Phys. Lett. B380 (1996) 205
14. K. Koller, T.F. Walsh, P.M. Zerwas, Z. Phys. C2 (1979) 197; E. Laermann, T.F. Walsh, I. Schmitt, P.M. Zerwas, Nucl. Phys. B207 (1982) 205
15. A. Gehrmann-De Ridder, E.W.N. Glover, DTP-97-24 (hep-ph/9705305); A. Gehrmann-De Ridder, T. Gehrmann, E.W.N. Glover, DTP-97-26 (hep-ph/9707224)
16. E.W.N. Glover, A.G. Morgan, Z. Phys. C62 (1994) 311
17. L. Bourhis, M. Fontannaz, J. Ph. Guillet, LPTHE-ORSAY-96-103 (hep-ph/9704447)
18. ALEPH Collaboration, D. Buskulic et al., Z. Phys. C69 (1996) 365; OPAL Collaboration, K. Ackerstaff et al., CERN-PPE-97-086 (subm. to Z. Phys. C)
19. Z. Kunszt, Z. Trocsanyi, Nucl. Phys. B394 (1993) 139; E.L. Berger, X. Guo, J. Qiu, Phys. Rev. D54 (1996) 5470; P. Aurenche et al., Phys. Rev. D55 (1997) 1124
20. H. Spiesberger et al., Workshop on Physics at HERA, Hamburg, Germany, Oct 29-30, 1991, p. 798
21. K. Charchuła, G.A. Schuler, H. Spiesberger, Comput. Phys. Commun. 81 (1994) 381
22. J.A.M. Vermaseren, Symbolic Manipulation with FORM, Amsterdam, 1991
23. D. Michelsen, PhD thesis, University of Hamburg, DESY 95-146
24. G. Altarelli, R.K. Ellis, G. Martinelli, Nucl. Phys. B143 (1978) 521; Nucl. Phys. B157 (1979) 461; W. Furmanski, R. Petronzio, Z. Phys. C11 (1982) 293; P.B. Arnold, M. Hall Reno, Nucl. Phys. B319 (1989) 37
25. K. Fabricius, G. Kramer, G. Schierholz, I. Schmitt, Z. Phys. C11 (1982) 315; W.T. Giele, E.W.N. Glover, Phys. Rev. D46 (1992) 1980
26. E. Mirkes, D. Zeppenfeld, Phys. Lett. B380 (1996) 205
27. P. Mättig, H. Spiesberger, W. Zeuner, Z. Phys. C60 (1993) 613
28. A.D. Martin, R.G. Roberts, W.J. Stirling, Phys. Rev. D51 (1995) 4756
29. M. Glück, E. Reya, A. Vogt, Z. Phys. C67 (1995) 433; H.H. Lai et al., CTEQ Collaboration, Phys. Rev. D51 (1995) 4763
30. H1 Collaboration, T. Ahmed et al., Phys. Lett. B346 (1995) 415; ZEUS Collaboration, M. Derrick et al., Phys. Lett. B363 (1995) 201